Earth and Planetary Science Letters 287 (2009) 205–216

Contents lists available at ScienceDirect

Earth and Planetary Science Letters

journal homepage: www.elsevier.com/locate/epsl

Source-side shear wave splitting and upper mantle flow in the Romanian Carpathians and surroundings

R.M. Russo [a,*], V.I. Mocanu [b,1]

[a] Dept. of Geological Sciences, P.O. Box 112120, 241 Williamson Hall, University of Florida, Gainesville, FL, 32611, USA
[b] Dept. of Geophysics, Bucharest University, 6 Traian Vuia St., RO-70139 Bucharest 1, Romania

ARTICLE INFO

Article history:
Received 2 April 2009
Received in revised form 27 July 2009
Accepted 2 August 2009
Available online 19 September 2009

Editor: L. Stixrude

Keywords:
Carpathians
Vrancea
shear wave splitting
upper mantle anisotropy
Transylvanian Basin
East European Platform

ABSTRACT

We present shear wave splitting measurements from 5 earthquakes that occurred in the Vrancea seismic zone of the Carpathian Arc. S waves from these events, all with magnitudes >5.4 M_w and deeper than 88 km, were recorded at broadband stations of the Global Seismic Network, and the Geoscope and Geofon Networks, and used by us to measure shear wave splitting corrected for sub-station splitting and anisotropy. In order to carry out these corrections we used published shear wave splitting parameters, thus isolating contributions to observed splitting from the Vrancea source region and upper mantle surrounding the Carpathian Arc. The resulting 32 good observations of source-side shear wave splitting, along with 54 null splitting observations (which yield two potential splitting directions) clearly show that upper mantle anisotropy is strongly variable in the region of the tightly curved Carpathian Arc: shear waves taking off from Vrancea along paths that sample the East and Southern Carpathians have fast anisotropy axes parallel to these ranges, whereas those leaving the source region to traverse the upper mantle beneath the Transylvanian Basin (i.e., mantle wedge side) trend NE–SW. Shear waves sampling the East European and Scythian Platforms are separable into two groups, one characterized by fast shear trends to the NE–SW, and a second, deeper group, with trends to NW–SE; also, the majority of null splits occur along paths leaving Vrancea in these NE–E azimuths. We interpret these results to indicate the presence of at least three distinct upper mantle volumes in the Carpathians region: the upper mantle beneath the Carpathian Arc is strongly anisotropic with fabrics parallel to the local arc strike; the Transylvanian Basin upper mantle fabrics trend NE–SW; and the anisotropy beneath the westernmost East European Platform may be characterized by a shallow NW–SE trending fabric concentrated in the cratonic lithosphere of the East European Platform, and a second, deeper fabric with E–W trend marking asthenospheric flow beneath the craton's base. This more complex anisotropy beneath the western edge of the East European Platform would account for both the variability of observed splitting of waves that sample this volume, and also the strong prevalence of nulls observed along eastward-departing azimuths.

1. Introduction

The Carpathian mountain chain in Romania is formed by two ranges, the East Carpathians, striking NNW, and the Southern Carpathians, which strike E–W (Fig. 1). The two meet in the Vrancea region, site of frequent, often high-magnitude seismicity at intermediate depths (70–220 km) (Oncescu and Bonjer, 1997). Vrancea zone seismicity occurs in a small volume, essentially a tabular structure with steep or vertical dip, whose ~70 km long axis trends NE–SW (Fig. 1). Inversion of travel times to permanent and temporary seismic stations situated above and around the Vrancea zone reveals a high seismic velocity (up to 5.8% fast) structure in the upper mantle striking NE–SW and extending near-vertically from 70 to 200 km depth, and from 200 to ~370 km depth with a more N–S strike (Martin et al., 2005; Weidle et al., 2005; Martin et al., 2006). Wortel and Spakman (2000) show the Vrancea high velocity body in contact with a deeper, high seismic velocity anomaly lying horizontally in the upper mantle transition zone, and interpret this body to be subducted lithosphere that once occupied the Transylvanian Basin region. Vrancea seismicity shallower than 70 km is rare, typically crustal, and of small magnitude (Radulian and Popa, 1996; Oncescu et al., 1999).

The East Carpathians appear to be a classic overthrust belt, verging eastwards, providing strong evidence that terranes of the Transylvanian Basin to the west of the range overrode and subducted Tethyan passive margin units at the leading edge of the East European Platform during the Miocene (e.g., Radulescu and Sandulescu, 1973; Csontos, 1995; Sandulescu, 1998; Wortel and Spakman, 2000; Sperner et al., 2001). Neogene volcanics outcropping on the western flanks of the

* Corresponding author. Tel.: +1 352 392 6766; fax: +1 352 392 9294.
E-mail addresses: rrusso@ufl.edu (R.M. Russo), mocanu@gg.unibuc.ro, vi_mo@yahoo.com (V.I. Mocanu).
[1] Tel.: +40 1 211 7390; fax: +40 1 211 3120.

0012-821X/$ – see front matter © 2009 Elsevier B.V. All rights reserved.
doi:10.1016/j.epsl.2009.08.028

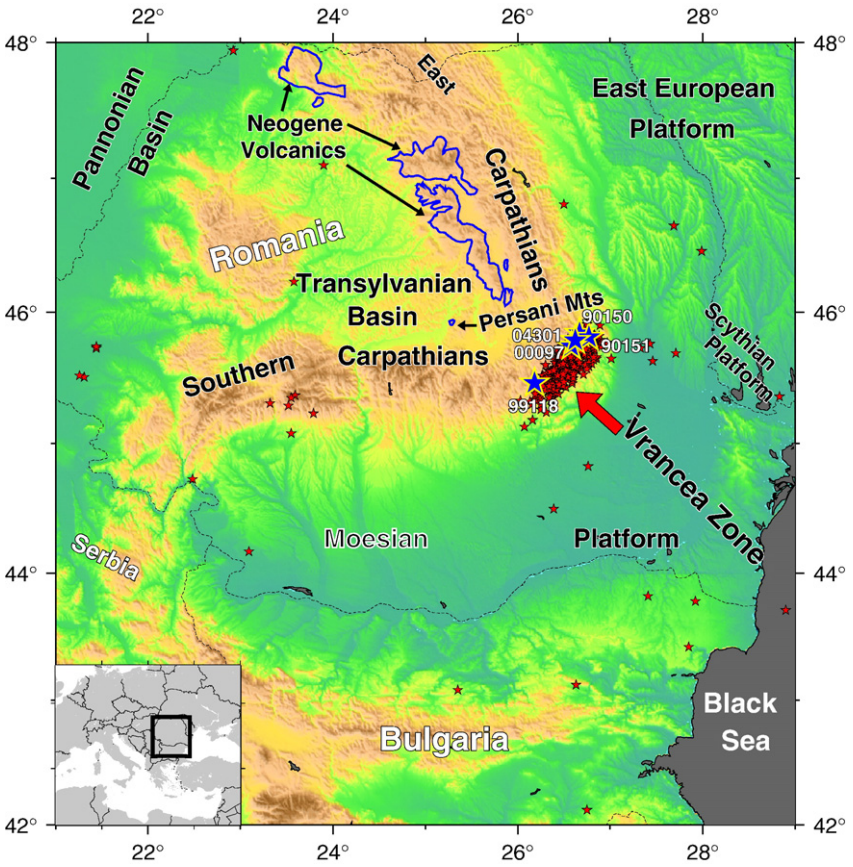

Fig. 1. Topography of the Carpathian arc, showing geography mentioned in text. Small red stars are background seismicity of the region, which defines the frequently active Vrancea zone (Romanian National Institute of Earth Physics catalog); large blue stars mark epicenters of 5 earthquakes used in this study. The Transylvanian Basin is composed of terranes that overrode an embayment of the Tethys Ocean during Cenozoic; Neogene volcanics are interpreted as suprasubduction arc lavas (e.g., Seghedi et al., 1998). Subduction was to the west beneath the East Carpathians (e.g., Sandulescu, 1998; Hippolyte et al., 1999); late Cenozoic motions along the South Carpathians were variable but mostly dextral strike-slip (e.g., Maţenco et al., 1997).

East Carpathians and into the adjacent Transylvanian Basin are consistent with formation as suprasubduction eruptives (Mason et al., 1998; Seghedi et al., 1998, 2004). In conjunction, the extant geologic structures of the East Carpathians and the associated volcanic units are consistent with westward subduction of oceanic Tethys or thinned passive margin lithosphere of the East European Platform beneath the Transylvanian Basin terranes (Linzer, 1996; Hippolyte et al., 1999; Ciulavu et al., 2000). In contrast, the Southern Carpathians are marked by south verging nappe structures internally (i.e., Transylvanian Basin side), but externally, south-tilted Moesian Platform sediments onlap the range front along its length, including the region adjacent to the Vrancea zone (Tărăpoancă et al., 2003), and late Cenozoic volcanics on the Transylvanian Basin side are absent, indicating that the Southern Carpathians structures were not formed by subduction. Evidence from structural analysis instead points to major dextral strike-slip with episodes of transpression and transtension during the Cenozoic (Linzer et al., 1998; Maţenco and Schmid, 1999; Dupont-Nivet et al., 2005; Maţenco et al., 2007).

The East and South Carpathians form a tightly curved arc, and the contrast between the origins and histories of the surrounding terranes — East European, Scythian, and Moesian Platforms to the east and south of the high Carpathians, and Transylvanian Basin terranes to the north and west — these ranges separate are pronounced. The cratonic East European Platform adjacent to the Carpathians, in particular, has a distinctive thick, cold lithosphere (Goes et al., 2000; Weidle et al., 2005) that transmits seismic energy efficiently (Russo et al., 2005; Weidle et al., 2007), whereas the lithosphere of the younger terranes on the Transylvanian Basin side of the Arc is thin (Lankreijer et al., 1997), and its upper mantle attenuates seismic waves strongly (Russo et al., 2005) and is relatively warm (Goes et al., 2000). Thus, the highly three-dimensional structure of the Carpathian Arc, and the differing natures of the surrounding continental masses implies that upper mantle anisotropic fabrics for this region should be highly heterogeneous. Available data from splitting of shear waves that traverse the Earth's core (e.g., *SK*(*K*)*S*) are few and widely spaced (Fig. 2) in the study region, and with few exceptions fast shear polarizations throughout Romania trend NW–SE, delay times ranging from 0.7 to 1.6 s (Ivan et al., 2008). Stations in the South Carpathians and Vrancea zone, however, have fast shear polarizations trending NE–SW (MLR, VOIR) or close to N–S (PLOR, VRI), although station VRI, situated above the eastern edge of the Vrancea seismic body and at the southern end of the East Carpathians, exhibits some variability in splitting parameters with source back azimuth, such that a subset of these data has NW–SE fast trends (Ivan et al., 2008). The South Carpathian–Vrancea zone station splitting results were interpreted by Ivan et al. (2008) to result from lithospheric fabrics formed by SE-directed collision between the Transylvania terranes and the Platform lithospheres east and south of the Carpathian Arc. Our goal in this paper is to augment the shear wave splitting data for the Vrancea zone and surroundings in order to gage the effects of late Cenozoic tectonics of this region on upper mantle fabrics. To do this, in the absence of more and closer-spaced seismic stations, we made use of larger magnitude earthquakes that occurred in the Vrancea zone and that were recorded at distant broadband seismic stations.

2. Data

Five Vrancea zone earthquakes attained sufficient magnitude to generate well-recorded S waves at teleseismic distance (Table 1).

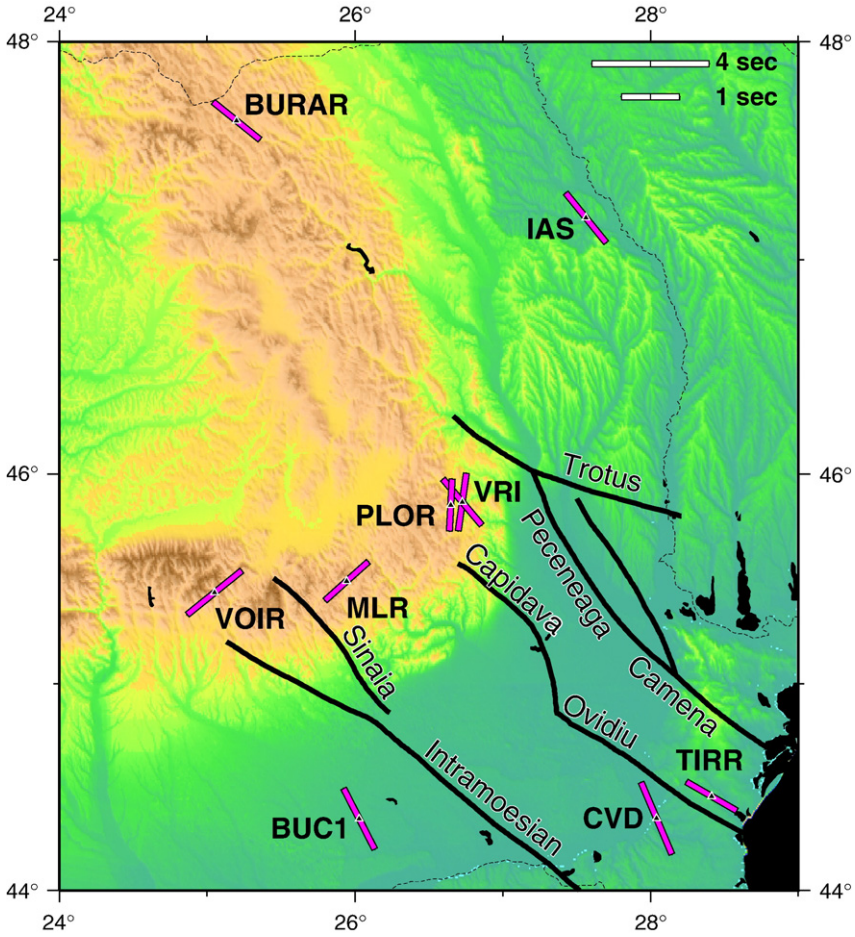

Fig. 2. Station shear wave splitting in the study region (Ivan et al., 2008). Fast shear trend parallel to bars, bar lengths scaled according to observed splitting delays. Traces of major faults of the Moesian and Scythian Platforms also shown.

Given a minimum depth of 88 km for these events (maximum 156 km), their S waves are easily separable from possible contamination by near-source surface reflections (*pS*, *sS*), and the main limitation on useful events is source magnitude; all the events we used have magnitudes > 5.4, as estimated by either the U.S. Geological Survey Earthquake Center or reported in the Global Centroid Moment Tensor Catalog. The events all lie within the recognizable boundaries of the Vrancea zone seismicity (Fig. 1), although four of the earthquakes occurred near the northeastern edge of the Vrancea zone, and one event ruptured the area close to its southwestern terminus.

Stations recording S waves from the five earthquakes are part of the IRIS Global Seismic Network (GSN), or the German Geofon or French Geoscope networks. Data for each event were downloaded from the IRIS Data Management Center (DMC), culled for quality (good signal-to-noise) and for appropriate distance for lower mantle turning points and to avoid cross-over with core shear phases ($30° < \Delta < 83°$). Although there are only five events, the broad coverage provided by these networks ensured that the upper mantle around the Vrancea source area was sampled in all azimuth quadrants. Thus, the regions below the main units mentioned above (East and South Carpathians; Transylvanian Basin; East European, Scythian, and Moesian Platforms) were all traversed by waves leaving the source area.

Table 1
Earthquake parameters.

Date	Julian day	Origin time	Latitude (°)	Longitude (°)	Depth (km)	Magnitude (M_w)
30 May 1990	150	10:40:06.10	45.841	26.668	89.0	7.1
31 May 1990	151	00:17:47.90	45.811	26.769	88.0	6.2
28 April 1999	118	08:47:55.40	45.464	26.183	156.0	5.4
06 April 2000	097	00:10:38.78	45.743	26.580	132.6	5.4
27 Oct. 2004	301	20:34:36.81	45.787	26.622	95.8	5.9

3. Method

In order to isolate source-side shear wave splitting we used published observations of *SK*(*K*)*S* splitting (see Supplementary Table 1, below) to characterize sub-receiver upper mantle anisotropy (Silver and Chan, 1991; Silver, 1996; and the Université de Montpellier shear wave splitting data base, www.gm.univ-montp2.fr/splitting/DB/). Given delay time and fast polarization angle, Φ_r for the recording station, S waves at the station can be corrected for receiver station upper mantle anisotropy. Receiver-side anisotropy is represented as the application of an operator, $\Gamma(\Phi_r,\delta t_r)$ (Russo and Silver, 1994; Russo, 2009, submitted for publication), and for an isotropic polarization vector $\hat{g}$ and wavelet function $w(\omega)$, the split shear wave $u_s(\omega)$ is:

$$u_s(\omega) = w(\omega)e^{[-i\omega T_0]}\Gamma(\Phi_r,\delta t_r)\cdot\hat{g} \quad (1)$$

where T_0 is the isotropic shear wave travel time and

$$\Gamma = e^{i\omega\delta t/2}\hat{a}\hat{a} + e^{-i\omega\delta t/2}\hat{s}\hat{s} \quad (2)$$

Here, $\hat{a}$ and $\hat{s}$ are unit vectors in the fast and slow polarization directions and Φ_r is the azimuth (clockwise from *N*) of $\hat{a}$. If both

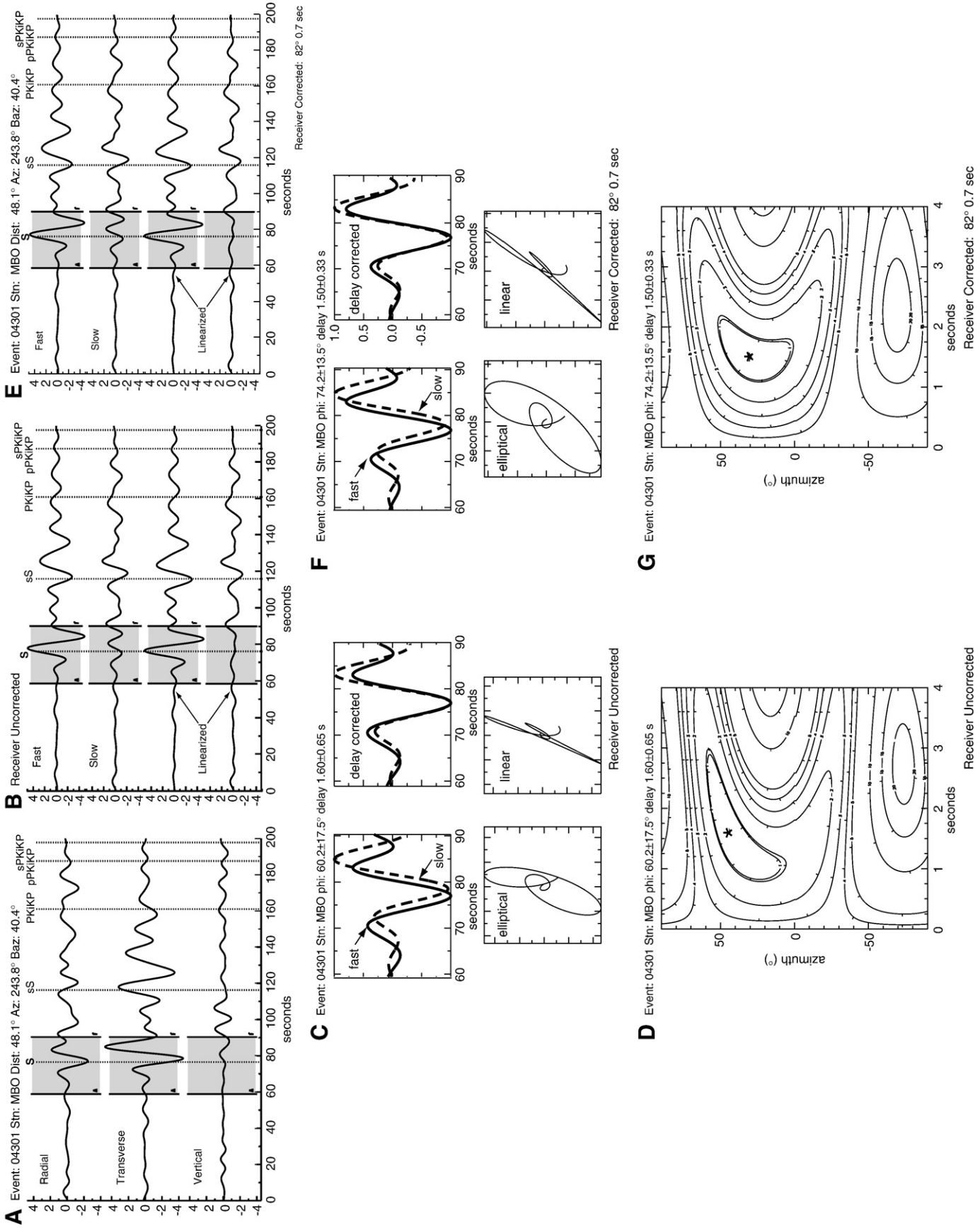

source and receiver splitting occur, we apply two operators, $\Gamma(\Phi_s,\delta t_s)$ (source) and $\Gamma(\Phi_r,\delta t_r)$ (receiver):

$$u_s(\omega) = w(\omega)e^{[-i\omega T_0]}\Gamma(\Phi_r,\delta t_r)\cdot\Gamma(\Phi_s,\delta t_s)\cdot\hat{g} \quad (3)$$

and if the receiver operator is known, then the source splitting parameters can be isolated by applying the inverse receiver operator, $\Gamma^{-1}(\Phi_r,\delta t_r)$:

$$u_s(\omega) = w(\omega)e^{[-i\omega T_0]}\Gamma^{-1}(\Phi_r,\delta t_r)\cdot\Gamma(\Phi_r,\delta t_r)\cdot\Gamma(\Phi_s,\delta t_s)\cdot\hat{g} \quad (4)$$

We rotated and time-shifted windowed S phases of variable duration (typically 10–20 s) according to the relevant station splitting, and also corrected resulting source-side splitting polarizations for the mirror-image reflection caused by passage from downward to upward propagation at the ray turning point. In many instances, the data were low-pass filtered prior to windowing and splitting estimation to enhance signal to noise, typically with corner frequency of 0.1 Hz. An example of the correction for receiver-side splitting is shown in Fig. 3. In some instances where no receiver station splitting parameters were available, uncorrected measurements that are similar to nearby corrected measurements were retained for further analysis. Typical source-side splitting is much stronger than that at stations (δt_r~1 s versus δt_s~2–3 s; Russo and Silver, 1994; Russo, 2009, submitted for publication), so splitting corrections are often relatively small.

Uncertainties in the station splitting parameters have only a limited effect on the corrections used to isolate source-side splitting. An example using the same data shown in Fig. 3 is shown in Fig. 4: source-side fast axes and delay times are slowly-varying functions of the receiver-side splitting corrections, at least in the vicinity of the uncertainty ranges of Φ_r and δt_r. Small changes in receiver delay time have a larger effect (~5°) on observed source-side splitting than do variations in station fast polarization azimuth, as expected given the relatively greater effect of time shifting the waveforms on the polarization. Typically, for a given station splitting delay time change (i.e., on the order of the reported delay time uncertainties, see Supplementary Table 1), calculated source-side fast polarization azimuths are remarkably stable, varying by less than 3° despite varying the station fast azimuths through a 20° range; source-side delay times may vary through a nominal range of $\pm$0.2–$\pm$0.4 s as the station fast axes are varied (e.g., Fig. 4). Thus, for the typical source-side splitting measurement shown in Fig. 3, for event 04301 as recorded at station MBO, station splitting parameter uncertainties yield a maximum change in the best source-side fast azimuths of less than 5°, and perhaps 0.5 s in delay time, on average. All receiver-corrected source-side splitting observations are detailed in Table 2. Details of the variation in splitting parameters as a function of receiver station correction are given in Supplementary Table 2. Results for each event, including nulls, are shown in map view in Fig. 5.

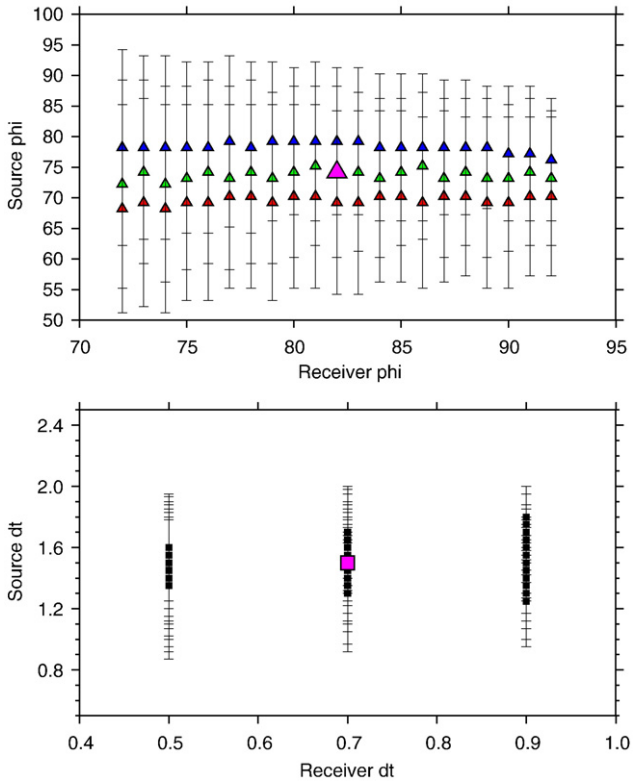

Fig. 4. Effect of station splitting parameter uncertainty on observed source-side splitting parameters. Data are for event 04301 recorded at MBO, as in Fig. 3. The station splitting measurement is taken from Russo and Silver (1994), $\Phi = 82° \pm 10°$, $\delta t = 0.7 \pm 0.2$ s. Both Φ and δt were varied through their reported uncertainty range (i.e., Φ from 72° to 92° by degree; δt was set to 0.5/0.7/0.9 s), and source-side splitting parameters were recalculated for each degree shift in station fast azimuth and each of the three delay times, yielding 63 source-side splitting estimations. The variability of δt_{src} with respect to δt_{rec} (bottom), and Φ_{src} and Φ_{rec} (top) were then plotted against each other. Φ_{src} symbols color coded according to δt_{rec}: red for 0.5, green for 0.7, and blue for 0.9 s. Large purple symbols mark the preferred published values used to make all other measurements involving station MBO. Φ_{src} is remarkably stable with respect to changes in Φ_{rec}, and varies more due to changes in δt_{rec}. Variation in δt_{src} due to uncertainty in receiver splitting parameters is more pronounced. (For interpretation of the references to color in this figure legend, the reader is referred to the web version of this article.)

4. Results

Splitting in the Carpathian Arc upper mantle is systematically variable (Fig. 5): S waves that leave the source region along NNW–NW azimuths — those that sample the region beneath the East Carpathians from ~90 km depth to the base of the olivine stability field (410 km) — have NNW-trending fast shear polarizations that parallel the strike of the East Carpathians, with one single exception. Measurements along paths sampling the region beneath the South Carpathians are far fewer, but here also, observed E-trending fast shear polarizations parallel the range strike. By far the largest number of observations are for paths that leave the source area along east or northeast azimuths, and sample the East European–Scythian Platforms upper mantle. Splitting along these paths falls into two groups, one with fast shear trends to the NNW, and a second with nearly orthogonal Φ trends to the ENE. A few measurements were made for paths traversing the Moesian Platform upper mantle, yielding N–S or

Fig. 3. A) Seismograms for shear wave of event 04301 rotated into radial-transverse directions. Gray areas mark splitting measurement window. B) 04301 shear waves rotated into fast-slow frame (top 2 traces) and linearized (bottom traces). No correction for receiver station anisotropy. C) Waveforms of 04301 shear waves in fast-slow frame (left) and after correcting for delay time (right). Note good waveform coherence (left), and linear particle motion after delay time correction (right). D) Splitting parameter grid search for station uncorrected 04301 splitting measurement. Best splitting parameters (fast shear azimuth and delay time) marked by star within double 95% confidence limit contour. Phi measurement reported in figure label corrected for polarization rotation due to propagation through shear wave turning point. E) 04301 shear wave splitting measurement corrected for splitting at receiver station MBO. Shear waves rotated into fast-slow frames (top 2 traces) and linearized (bottom traces). Gray areas mark splitting measurement window. F) Receiver corrected waveforms of 04301 shear waves in fast-slow frame (left) and after correcting for delay time (right). Note improved waveform coherence. Bottom panels show elliptical particle motion before delay-time correction (left), and linear particle motion after delay time correction (right). G) Splitting parameter grid search for 04301 splitting measurement corrected for MBO station splitting. Best splitting parameters (fast shear azimuth and delay time) marked by star within double 95% confidence limit contour. Phi measurement reported in figure label corrected for polarization rotation due to propagation through shear wave turning point.

Table 2
Splitting measurements.

Station	Δ (°)	Azimuth (°)	Back azimuth (°)	Polarization (°)	Φ (°)	Φ uncertainty (°)	δt (s)	δt uncertainty (s)
30 May 1990 (90150)								
ALE	44.7	349.2	83.1	−70.99	117	7	1.95	0.30
BJI	62.3	60.1	308.0	−0.13	160	5	3.45	0.20
CAY	78.9	265.6	44.3	1.22	129	5	null	
CCM	79.6	314.9	38.8	37.22	167	14	1.45	0.35
ERM	75.7	43.6	319.8	−35.75	12	9	2.00	0.38
HIA	58.8	49.9	305.4	−12.84	153	8	2.35	0.25
HRV	66.0	306.8	49.1	49.73	165	11	2.60	0.35
INU	77.6	51.8	317.9	4.69	133	8	2.60	0.28
MBO	48.3	243.9	40.3	−27.09	98	9	2.35	0.28
SCP	70.6	308.9	45.7	46.31	5	11	1.80	0.30
TSK	78.6	49.3	319.2	9.04	151	3	3.70	0.15
WFM	65.9	306.8	49.2	46.4	156	16	2.60	0.60
31 May 1990 (90151)								
ALE	44.8	349.3	84.0		72	7	2.10	0.18
BJI	62.4	62.4	307.9	−22.2	130	2	2.45	0.40
CCM	79.7	314.9	38.9	−31.7	26	23	Null	
ERM	75.8	43.5	319.7	−38.6	42	23	Null	
HIA	58.9	49.8	305.4	−23.6	25	23	Null	
HRV	66.0	306.8	49.2	−31.0	27	23	Null	
INU	77.7	51,7	317.8	−26.0	35	17	Null	
LZH	56.9	70.4	305.6	−85.7	141	11	2.75	0.45
WMQ	42.9	69.4	294.9		141	18	1.65	0.38
28 April 1999 (99118)								
AAK	34.4	77.1	291.6	−79.4	88	23	Null	
ASCN	64.4	225.6	30.5	7.0	69	23	Null	
ATD	36.7	151.9	340.3	−39.4	82	23	Null	
BJT	62.9	59.6	307.8	−67.7	75	23	Null	
BORG	32.3	323.7	103.5	−42.0	19	23	Null	
ENH	64.7	71.9	309.4	−70.3	2	23	Null	
LSA	52.4	83.8	306.5	−51.0	81	23	Null	
MDJ	67.6	48.7	312.2	−74.5	75	7	Null	
28 April 1999 (99118)								
MSEY	56.3	144.1	335.6	−34.7	172	5	3.95	0.57
SJG	78.9	284.5	45.8	79.0	71	23	Null	
TLY	49.4	53.2	295.2	−67.4	78	7	4.00	0.45
WUS	38.2	77.0	294.7	−56.1	97	17	2.90	0.57
ULN	53.1	56.2	299.7	−70.6	67	10	Null	
XAN	62.0	68.9	307.7	−47.4	84	9	2.90	0.60
06 April 2000 (00097)								
AAK	34.1	77.7	292.0	−5.3	15	23	Null	
BJT	62.5	59.9	307.9	34.9	63	23	Null	
COLA	69.6	357.5	4.1	10.7	152	13	Null	
FFC	70.8	331.3	35.4	−23.6	142	5	2.90	0.45
HIA	59.1	49.7	305.4	23.7	61	23	Null	
KURK	34.4	62.5	282.4	2.8	72	23	Null	
LSA	52.1	84.3	306.8	36.6	84	23	Null	
MA2	65.5	27.6	320.5	32.7	45	23	Null	
MAKZ	56.9	70.4	305.6	−15.4	174	12	2.72	0.68
SFJ	44.2	326.6	78.6	−83.6	141	21	1.50	1.00
TIXI	51.0	23.5	298.2	4.5	106	8	Null	
TLY	49.0	53.5	295.2	7.3	71	23	Null	
YAK	56.3	33.5	304.9	31.7	141	5	4.00	0.63
27 October 2004 (04301)								
AAK	34.1	77.8	292.1	−29.3	39	23	Null	
ALE	44.8	349.6	83.4	−58.2	41	23	Null	
ASCN	64.8	225.9	30.5	−56.7	43	2	Null	
ATD	36.8	152.8	341.0	10.8	33	23	Null	
BJT	62.5	60.0	307.9	31.2	67	23	Null	
BORG	32.2	323.3	102.7	−84.7	47	2	4.00	0.22
CCM	79.6	314.8	39.0	40.7	43	23	Null	
CHTO	64.5	88.8	312.4	46.4	74	8	3.65	1.18
ENH	64.3	72.3	309.6	35.9	64	2	3.35	0.35
ERM	75.9	43.4	319.8	31.9	72	5	2.10	0.55
FURI	38.2	160.5	346.3	39.5	39	6	4.00	0.60
HIA	59.0	49.7	305.4	22.2	63	23	Null	

Table 2 (*continued*)

Station	Δ (°)	Azimuth (°)	Back azimuth (°)	Polarization (°)	Φ (°)	Φ uncertainty (°)	δt (s)	δt uncertainty (s)
27 October 2004 (04301)								
HRV	66.0	306.7	49.3	47.1	39	23	Null	
KMBO	47.7	165.5	349.9	44.2	21	23	Null	
KMI	63.0	81.0	310.3	41.5	80	23	Null	
LBTB	70.5	181.0	0.8	77.8	14	23	Null	
LSZ	60.8	178.3	358.7	78.2	29	16	2.70	0.68
MA2	65.5	27.6	320.5	28.6	49	23	Null	
MAJO	77.5	318.2	318.2	23.2	65	6	3.85	1.13
MBAR	46.3	174.3	356.0	64.8	51	10	2.50	0.28
MBO	48.1	243.8	40.4	−21.7	74	14	1.50	0.33
MDJ	67.2	49.0	312.3	−58.4	60	1	Null	
MSEY	56.4	144.7	336.1	−11.3	42	23	Null	
QIZ	72.0	81.1	313.1	45.1	79	23	Null	
RSSD	80.4	326.3	32.6	56.4	131	2	3.45	0.45
SSE	71.4	64.5	312.6	49.7	57	23	Null	
SSPA	70.7	308.7	45.9	52.7	32	23	Null	
TATO	75.8	68.9	314.0	43.7	69	23	Null	
TIXI	50.9	23.5	298.2	9.1	43	23	1.80	0.38
ULN	52.7	56.6	299.8	20.9	47	8	Null	
WMQ	42.5	69.8	294.9	15.3	79	23	Null	
YAK	56.3	33.5	304.9	17.9	50	4	Null	
YSS	72.0	40.3	318.7	28.9	60	23	Null	

NE–SW fast shear trends, and a single path sampling the upper mantle beneath the Transylvanian Basin produced a measurement with Φ trending NE–SW. In all, we made 32 measurements of source-side shear wave splitting from the five Vrancea earthquakes.

Fig. 5 also shows the 54 null splitting observations produced by our analyses. The nulls, which indicate that either no upper mantle anisotropy is present, or the initial shear polarization is fortuitously parallel to either the along-path fast or slow anisotropic symmetry axes, are remarkably consistent with the splitting along similar paths: one of the two potential fast shear directions for each null parallels the observed fast shear polarization direction of nearby measurements. Note that the null splitting observations are also consistent between events, and they expand the sampling of the study region upper mantle by augmenting the azimuthal coverage.

5. Discussion

5.1. Splitting source at depth

Based on the clear similarity between our source-side splitting measurements and core phase splitting at *most* stations in the study region (Fig. 6), several conclusions can be drawn: First, very heterogeneous upper mantle anisotropy is unlikely, since the splitting for both data sets is similar over regional distances and consistent within the upper mantle beneath the major tectonic units. A possible exception to this notion is that anisotropy in the immediate vicinity of the Vrancea high velocity body could be very heterogeneous based on observations of variable anisotropy at stations situated above the body (Ivan et al., 2008), although the volume of such material would necessarily have to be small so as not to affect observations on a wide scale. The analysis of splitting variation with changing anisotropic symmetry along path modeled by Saltzer et al. (2000) leads to the expectation that observed apparent splitting of downgoing S waves would be imprinted by the last (deepest) upper mantle anisotropy encountered by the waves, whereas the apparent splitting for upward-traveling *SK*(*K*)*S* waves would reflect the shallowest anisotropy encountered by those waves. Since the two data sets are similar, either the fabric of the entire upper mantle from surface to the 410 km discontinuity is similar (vertical coherence of anisotropic fabrics, e.g., Silver, 1996), or the deeper portion of the upper mantle from 90 to 410 km is strongly anisotropic with consistently oriented fabrics, and the shallow, lithospheric portions of the region are only very weakly anisotropic. The SKS splitting results of Ivan et al. (2008) integrate all anisotropy from the base of the olivine stability field to the surface, but given the strong source-side splitting along upper mantle paths from 90 km depth and deeper, the similarity between the observations indicates that the principal anisotropic source of splitting lies deeper than 90 km. Similarly, large volumes of upper mantle deeper than 90 km cannot have pervasive vertical or steeply plunging anisotropy (despite the obviously rapid vertical sinking of Vrancea body material), since such anisotropies would yield no splitting for the downgoing S phases, contrary to observations. Also, given fairly high (0.7–1.6 s) splitting delay times for the *SK*(*K*)*S* phases, and source-side splitting delay times ranging from 1.45 to 4 s (mean 2.77 s), large volumes of isotropic upper mantle are also ruled out. We conclude that the principal source of anisotropy here resides in the asthenosphere, or that lithospheric fabrics parallel those in the deeper upper mantle but contribute relatively little to observed splitting. Note also that the similarity between the strikes of the East and South Carpathians (e.g., surface geology) and the upper mantle fabrics delineated by the source-side splitting seems to imply coaxial deformation fabrics from surface down to at least asthenospheric upper mantle depths, and certainly deeper than the ~90 km depths of the source events we used.

5.2. Splitting and seismic anisotropy

We rule out explanations of the observed splitting measurements that entail single, widespread plunging anisotropies (e.g., Chevrot and van der Hilst, 2003) beneath the Carpathians, since the observed variation of splitting fast directions with source–receiver azimuth does not fit the expected 2π periodicity such anisotropies would produce (Fig. 7). Thus, we invoke the most common interpretation of teleseismic shear wave splitting, based on development of linear preferred orientation of natural upper mantle minerals, predominantly olivine, with a tendency for aggregates of these minerals to align in the shear plane parallel to the direction of tectonic extension (Christensen, 1984; Nicolas and Christensen, 1987; Ribe, 1989a,b; Ribe and Yu, 1991; Zhang and Karato, 1995; Zhang et al., 2000). Laboratory experiments on natural and synthetic aggregates representative of dry upper mantle compositions indicate that when such rocks yield shear wave splitting, observed fast polarization directions parallel the [100] crystallographic axes of the aligned minerals (e.g., Hess, 1964; Carter et al., 1972; Kaminsky and Ribe, 2001), the type-A

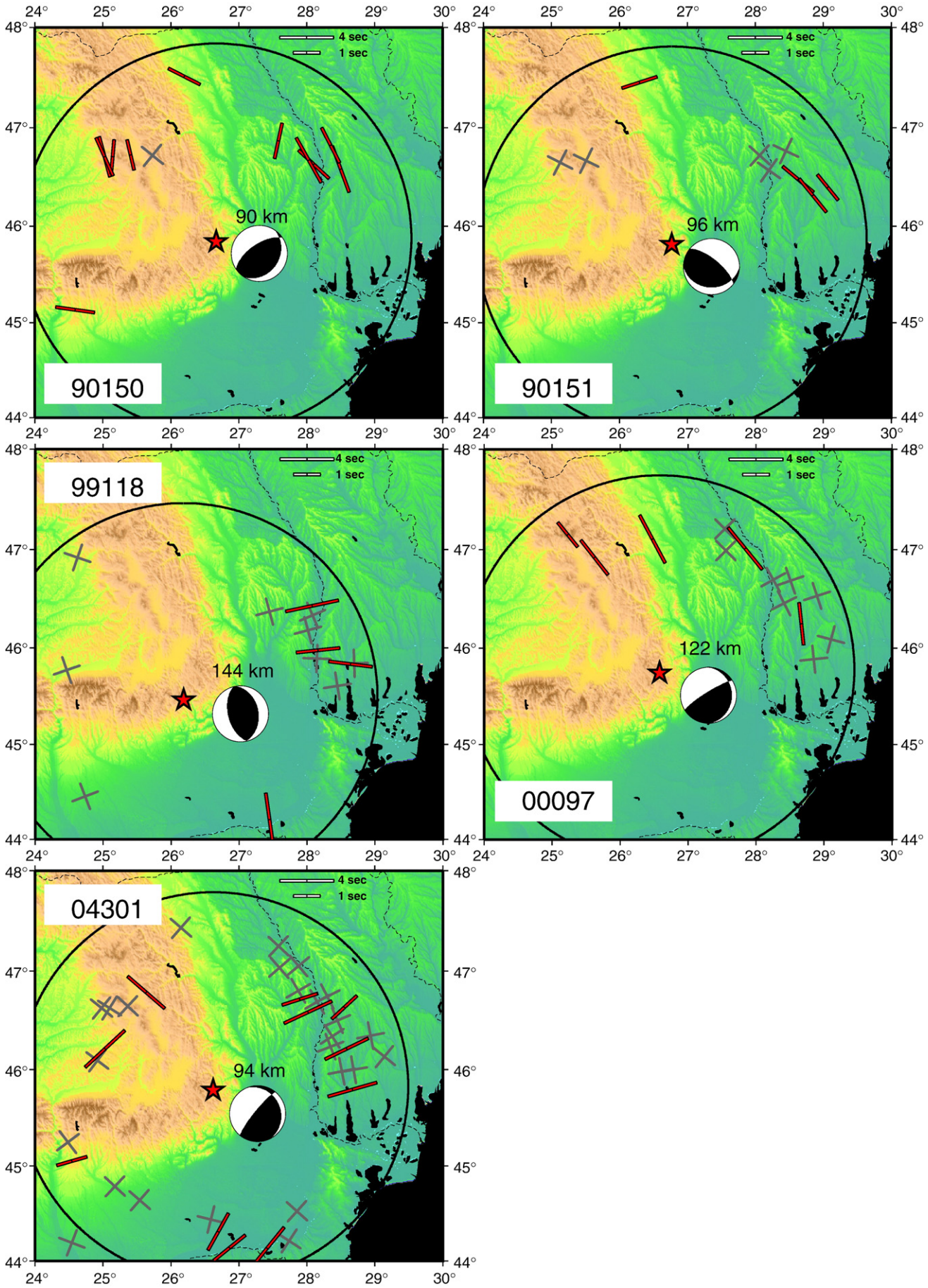

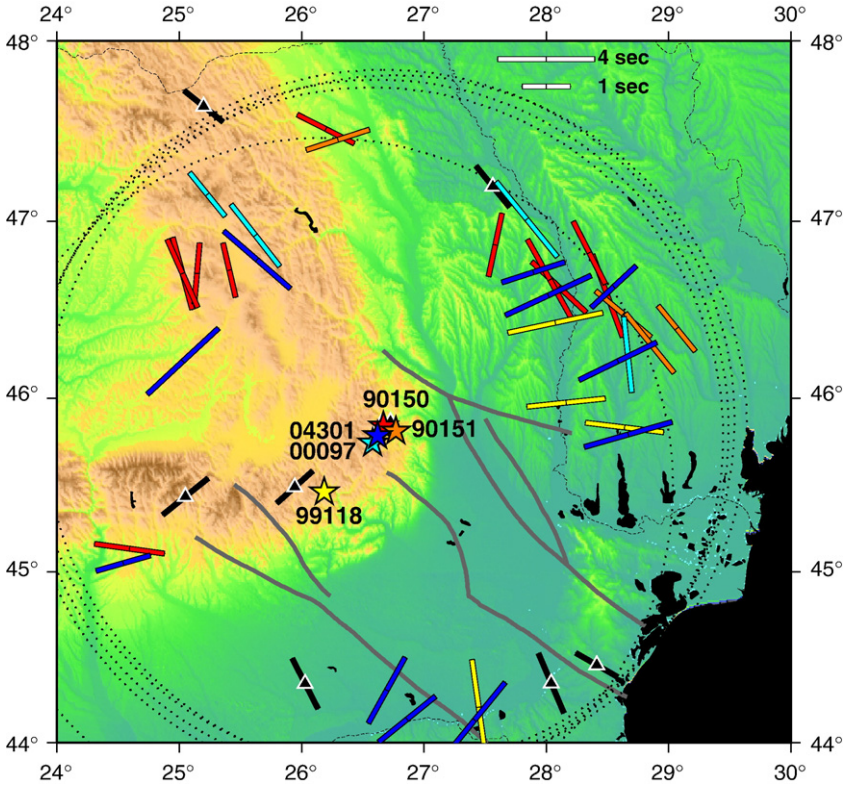

Fig. 6. Source-side shear wave splitting results from all 5 study earthquakes, event location (stars) and split (bars) color coded to match. Gray dotted circles are surface projections of 2° radius lower focal hemispheres for reference. Splits plotted at surface projections of 200 km depth piercing points along event-station ray paths to show geometry of sampling for individual event-station pairs. Splitting delay times as per key, upper right. Black bars with white-bordered triangles are splitting from *SK(K)S* phases at stations in the study region (Ivan et al., 2008).

fabric of Jung et al. (2006). Compilations of natural upper mantle samples from locales around the globe indicate that the predominant form of upper mantle anisotropy follows this basic type-A fabric (Mainprice and Silver, 1992; Ben Ismail and Mainprice, 1998). Jung et al. (2006) also note the existence of type-C and type-E fabrics which are petrographically distinct but which yield shear wave splitting with fast polarizations in the material flow direction similar to that produced by the A-type fabric (see their Fig. 12).

5.3. Splitting and upper mantle deformation

Observed parallelism of *SK(K)S* (Ivan et al., 2008) and source-side S fast splitting polarizations and also the strike of compressional structures of the East Carpathians (Fig. 6) indicate that the anisotropic fabrics at depth beneath this range are similar to the surface deformation fabrics (e.g., Nicolas, 1993; Silver 1996; Bendick and Flesch, 2007). Two possible scenarios for the formation of these fabrics are viable: 1) the fabrics formed perpendicular to the maximum compressive stress during shortening of the East Carpathians and collision with the EEP; or, 2) upper mantle flow parallel to the East Carpathians strike from NW to SE occurred as the subducted Tethyan lithosphere beneath the Transylvania Basin tore off the leading edge of the EEP and sank in to the mantle (Wortel and Spakman, 2000). Support for the latter scenario comes from the observed time progression of Neogene eruptives (Fig. 1) along the East Carpathians, which are older to the NW and young to the SE (Seghedi et al., 1998). That these splitting measurements might be due to a frozen lithospheric anisotropic fabric is less likely, given observed high upper mantle temperatures beneath the East Carpathians (Goes et al., 2000), and clear observations of high attenuation along paths from Vrancea earthquakes to stations in the East Carpathians (Russo et al., 2005).

Thus, these upper mantle fabrics were produced during late Cenozoic deformation of the East Carpathians and the depth of our sampling demonstrates that they arise in the asthenospheric mantle, but the influence of pre-existing structures of the East European Platform on the collision between Transylvanian Basin terranes and the EEP likely was the controlling factor in deformation fabric development at upper mantle depths all along the collision zone. In particular, the Tornquist–Teisseyre zone (TTZ) structure, which bounds the Platform on the west and marks the western limit of thick East European cratonic lithosphere (e.g., Guterch et al., 1986; Pharaoh, 1999; Goes et al., 2000; Plomerová et al., 2002; Babuška and Plomerová, 2004), very probably provided the buttressing element that oriented late Cenozoic East Carpathians upper mantle fabrics and surface deformation, but the TTZ itself is characterized by much older preserved anisotropic fabrics that trend NW–SE along its extraordinary length from the Carpathians region into Scandinavia.

Sampling of the upper mantle beneath the EEP itself or along its western edge (Fig. 6) reveals two nearly distinct groups of splitting measurements, one with fast shear trends to the NW–SE, parallel to edge of the EEP (i.e., the TTZ) and sampled by shallower rays, and a second group with E–W fast axes which samples a region slightly nearer the Vrancea zone (Fig. 8). We thus consider two different

Fig. 5. Source-side splitting measurements (red bars trending in fast shear direction, length scaled by delay time, key upper right) and nulls (gray crosses, oriented in allowed fast shear trends) for each of the 5 study earthquakes. Harvard CMT focal mechanisms shown at epicenter, hypocentral depth indicated. Splitting and nulls plotted at surface projections of 200 km deep piercing points along event-station ray paths; black circles are mark of surface projection of 2° lower focal hemisphere, for comparison. The shear waves sample the strongly 3-D Carpathian Arc and surroundings in a highly variable fashion. (For interpretation of the references to color in this figure legend, the reader is referred to the web version of this article.)

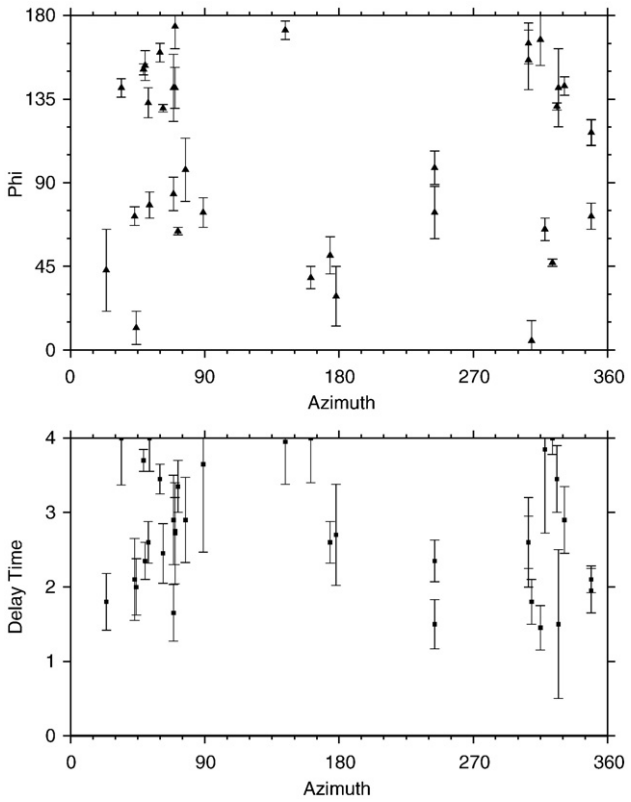

Fig. 7. Variation of observed source-side splitting parameters with event-station azimuth for φ (top) and δt (bottom). Note the φ trends in particular cannot be fit by a sinusoid with 2π periodicity, as would be expected for splitting due to a single plunging anisotropic fabric.

anisotropic fabrics residing either adjacent to each other, one a bit west of the other lying along the TTZ, or perhaps juxtaposed along the east-dipping base of the EEP. Note that the EEP thickens eastward rapidly in this region (Goes et al., 2000), and thus the eastern, NW–SE trending splitting may be due to ancient lithospheric fabrics entirely within the EEP (e.g., TTZ), whereas the western, E–W splitting represents asthenospheric flow west of, and below, the EEP. Such flow could be either westward, entrained by the Vrancea high velocity body sinking; or eastward, propelled by rollback of the Vrancea high velocity body, and displacing asthenospheric upper mantle to the east and downward, guided by the eastward thickening of EEP craton. We prefer the latter scenario, as it can also explain the high proportion of null splitting observations for ray paths to the east (see Section 5.4 below).

In contrast to the observations in the East Carpathians and EEP, the few source-side splitting and *SK*(*K*)*S* splitting observations in the South Carpathians are not parallel (Fig. 6). Instead, we find E–W (range parallel) fast shear trends for two measurements that sample upper mantle beneath and just south of the South Carpathians, but splitting at two stations situated in the South Carpathians has NE–SW fast trends. The latter are instead similar to the single source-side splitting measurement we made for a path that samples the Transylvanian Basin upper mantle (Fig. 6). A possible interpretation consistent with all observations is that upper mantle fabrics beneath the northern South Carpathians and Transylvanian Basin trend NE–SW, parallel to the long axis of the Vrancea high seismic velocity body at upper mantle depths down to 200 km (Martin et al., 2005; Weidle et al., 2005; Martin et al., 2006) and perpendicular to the south-eastwards trajectory of overriding Transylvanian Basin terranes in models of late Cenozoic collision between the terranes and surrounding Platform lithospheres (e.g., Ciulavu et al., 2000; Ivan et al., 2008). The E–W source-side splits sample the southern portion of the South Carpathians and northernmost Moesian Platform upper mantle, and may reflect strain partitioning into fabrics developed in compressional collision on the Transylvanian Basin side (e.g., NE–SW) and the more strike-slip dominated deformation (E–W) of the South Carpathians at more southerly latitudes.

Splitting fast trends to the south of the study region, along paths that sample the Moesian platform (Fig. 6) are variable. *SK*(*K*)*S* splits at two stations appear close to paralleling nearby major strike-slip

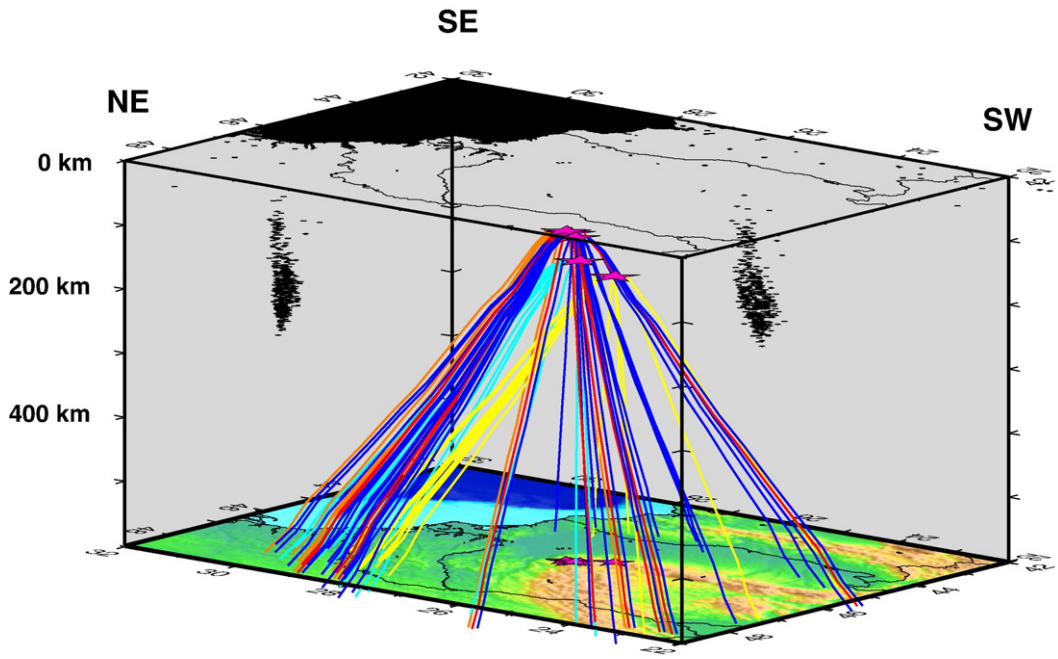

Fig. 8. Raypaths from 5 study earthquakes to distant stations where shear waves were recorded. Rays from each event color coded: red = 90150, orange = 90151, yellow = 99118, cyan = 00097, and blue = 04301. Note rays from the events sample the upper mantle beneath the East and South Carpathians, the Transylvanian Basin, and the East European, Scythian, and Moesian Platforms. Even taking into account Fresnel zones for the S waves, the image demonstrates that they sample heterogeneous structure, and therefore may experience different upper mantle anisotropic fabrics. Black squares on east and south box walls are projections of Vrancea Zone hypocenters, showing distribution of that seismicity. View from the NW looking SE.

faults (Ivan et al., 2008), but observations at a third station do not conform to this pattern. Fast shear polarizations at three of our source-side splitting measurements trend NE–SW, and a fourth trends N–S. These directions do not obviously relate to any known upper mantle structures.

5.4. Null splitting

Strong splitting (mean delay time is 2.77 s) is frequently observed at a given station even though the S wave for a given event at a neighboring station is null. The S wave travel paths for these stations are very similar, so it is unlikely, given Fresnel zone estimates for waves with periods >10 s (e.g., Zhao et al., 2000), that the study region upper mantle includes large-scale isotropic pockets. Note also that in some instances stations recording null splitting for one Vrancea event show clear splits for another. Splitting nulls result from a combination of focal mechanism initial S wave polarization (nodal for S radiation); source–receiver and anisotropic symmetry geometries; and event source complexity, which complicates waveforms and may change initial polarization; potentially because of subtle errors in receiver station corrections; because of suppression of the split signal by attenuation either in the source region (e.g., Transylvanian Basin), or somewhere along the travel path to the station; and, for the Vrancea zone especially, possibly due to complex heterogeneous anisotropy somewhere along path. Nonetheless, the observed source-side splitting is largely consistent between the five events. A group of splitting nulls (Fig. 5) visible along paths that sample the upper mantle to the east of Vrancea may also be due in part to a mild eastward plunge of the anisotropic fabrics beneath the western EEP craton.

5.5. Possible deeper structures

At the deepest upper mantle levels, known structures appear to bear little relation to the observed source-side splitting results. Martin et al. (2005, 2006) report that the long axis of the high seismic velocity anomaly beneath Vrancea strikes NE–SW down to 200 km depth, but then rotates to a more N–S strike between 200 and 370 km beneath the surface. Virtually none of the source-side splitting fast directions trend N–S. Also, Wortel and Spakman (2000) resolved what appears to be a continuation of this high velocity anomaly lying horizontally in the mantle transition zone beneath the Transylvanian and Pannonian Basins. Assuming this seismic anomaly is subducted Tethyan lithosphere, as indicated by Wortel and Spakman (2000), the effect of such a recumbent structure on splitting of shear waves that traverse it would depend strongly on the degree to which that lithosphere had developed an anisotropic fabric during its formation at an oceanic spreading ridge, and also on the degree to which such fabrics were preserved after subduction to transition zone depths. Anisotropic fabrics of typical oceanic lithosphere yield shear wave splitting with fast directions paralleling transform faults and fracture zones which offset the lithosphere-generating spreading ridges, and delay times are typically around 2 s (Russo and Okal, 1998; Garcia and Russo, 2005). The Tethyan lithosphere that occupied the Pannonian and Transylvanian Basins prior to the late Cenozoic is completely subducted, and hence the orientations of any such fabrics — if preserved at all today — are speculative at best. We see no clear evidence for a systematic contribution to splitting of waves that traverse this part of the study region mantle.

6. Conclusions

Source-side shear wave splitting from 32 measurements deriving from 5 Vrancea zone earthquakes reveal a systematic variability in upper mantle anisotropy beneath the Romania Carpathians and surroundings. These splitting measurements were corrected for shear wave splitting due to upper mantle anisotropy beneath the distant recording stations using published shear wave splitting parameters. Ray tracing to determine the upper mantle volumes sampled by the S waves leaving the source region allows us to ascribe highly variable shear wave splitting to different regions, yielding results consistent with other studies of shear wave splitting (Ivan et al., 2008) and upper mantle thermal state (Goes et al., 2000; Russo et al., 2005). Given source events in the Vrancea zone occurring at depths greater than 88 km, the clear relationship between our results and surface geology in the East and South Carpathians implies that anisotropic fabrics paralleling these ranges extend well below the lithosphere and almost certainly reside in the asthenosphere. Upper mantle fabrics beneath the East European Platform form two distinct group, one, lying to the east within the cratonic lithosphere of the EEP, characterized by NW–SE fast shear axes that parallel the Tornquist–Teisseyre zone; and a second, more westerly anisotropy that may represent asthenospheric flow to the east beneath the EEP lithosphere.

Acknowledgments

An early version of this work was supported by National Science Foundation grant EAR-0230336. We are very grateful to Editor Lars Stixrude and two anonymous reviewers whose cogent and thorough comments helped us improve this work.

Appendix A. Supplementary data

Supplementary data associated with this article can be found, in the online version, at 10.1016/j.epsl.2009.08.028.

References

Babuška, V., Plomerová, J., 2004. The Sorgenfrei–Tornquist zone as the mantle edge of Baltica lithosphere: new evidence from three-dimensional seismic anisotropy. Terra Nova 16, 243–249.
Ben Ismail, W., Mainprice, D., 1998. An olivine fabric database: an overview of upper mantle fabrics and seismic anisotropy. Tectonophysics 296, 145–157.
Bendick, R., Flesch, L., 2007. Reconciling lithospheric deformation and lower crustal flow beneath central Tibet. Geology 35, 895–898.
Carter, N., Baker, D., George, R., 1972. Seismic anisotropy, flow and constitution of the upper mantle. In: Heard, H., Borg, I., Carter, N., Raleigh, C. (Eds.), Flow and Fracture of Rocks. Geophys. Mono., vol. 16. Amer. Geophys. Union, Washington, DC, pp. 167–190.
Chevrot, S., van der Hilst, R., 2003. On the effects of a dipping axis of symmetry on shear wave splitting measurements in a transversely isotropic medium. Geophys. J. Int. 152, 497–505.
Christensen, N.I., 1984. The magnitude, symmetry and origin of upper mantle anisotropy based on fabric analyses of ultramafic tectonics. Geophys. J. R. Astron. Soc. 76, 89–112.
Ciulavu, M., Dinu, C., Szakács, A., Dordea, D., 2000. Neogene kinematics of the Transylvanian Basin (Romania). Am. Assoc. Pet. Geol. Bull. 84, 1589–1615.
Csontos, L., 1995. Tertiary tectonic evolution of the intra-Carpathians area: a review. Acta Vulcanol. 7, 1–13.
Dupont-Nivet, G., Vasiliev, I., Langereis, C.G., Krijgsman, W., Panaiotu, C., 2005. Neogene tectonic evolution of the southern and eastern Carpathians constrained by paleomagnetism. Earth Planet. Sci. Lett. 236, 374–387.
Garcia, T.M., Russo, R.M., 2005. Mantle flow beneath the Pacific Basin determined via shear wave splitting. Eos, Trans. — Am. Geophys. Union 86 (52) Fall Meeting Suppl., Abstract T23A-0525.
Goes, S., Govers, R., Vacher, P., 2000. Shallow mantle temperatures under Europe from P and S wave tomography. J. Geophys. Res. 105, 11,153–11,169.
Guterch, A., Grad, M., Materzok, R., Perchuc, E., 1986. Deep structure of the Earth's crust in the contact zone of the Paleozoic and Precambrian platforms in Poland (Tornquist–Teissere Zone). Tectonophysics 128, 251–279.
Hess, H.H., 1964. Seismic anisotropy of the uppermost mantle under oceans. Nature 203, 629–631.
Hippolyte, J.C., Badescu, D., Constantin, P., 1999. Evolution of the transport direction of the Carpathian belt during its collision with the East European Platform. Tectonics 18, 1120–1138.
Ivan, M., Popa, M., Ghica, D., 2008. SKS splitting observed at the Romanian broadband seismic network. Tectonophysics 462, 89–98.
Jung, H., Katayama, I., Jiang, Z., Hiraga, T., Karato, S., 2006. Effect of water and stress on the lattice-preferred orientation of olivine. Tectonophysics 421, 1–22.
Kaminsky, E., Ribe, N., 2001. A kinematic model for recrystallization and texture development in olivine polycrystals. Earth Planet. Sci. Lett. 189, 253–267.
Lankreijer, A., Mocanu, V.I., Cloetingh, S., 1997. Lateral variation in lithospheric strength in the Romanian Carpathians: constraints on basin evolution. Tectonophysics 272, 269–290.

Linzer, H.-G., 1996. Kinematics of retreating subduction along the Carpathian arc, Romania. Geology 24, 167–170.
Linzer, H.-G., Frisch, W., Zweigel, P., Girbacea, R., Hann, H.-P., Moser, F., 1998. Kinematic evolution of the Romanian Carpathians. Tectonophysics 297, 133–156.
Mainprice, D., Silver, P.G., 1992. Constraints on the interpretation of teleseismic SKS observations from kimberlite nodules from the subcontinental mantle. Phys. Earth Planet. Inter. 78, 257–280.
Martin, M., Ritter, J.R.R., CALIXTO Working Group, 2005. High-resolution teleseismic body-wave tomography beneath SE Romania — I. Implications for three-dimensional versus one-dimensional crustal correction strategies with a new crustal velocity model. Geophys. J. Int. 162, 448–460.
Martin, M., Wenzel, F., CALIXTO Working Group, 2006. High-resolution teleseismic body-wave tomography beneath SE Romania — II. Imaging of a slab detachment scenario. Geophys. J. Int. 164, 579–595.
Mason, R.D., Seghedi, I., Szakács, A., Downes, H., 1998. Magmatic constraints on geodynamic models of subduction in the East Carpathians, Romania. Tectonophysics 297, 157–176.
Maţenco, L., Schmid, S., 1999. Exhumation of the Danubian nappes system (South Carpathians) during the Early Tertiary: inferences from kinematic and paleostress analysis at the Getic/Danubian nappes contact. Tectonophysics 314, 401–422.
Maţenco, L., Zoetemeijer, R., Cloetingh, S., Dinu, C., 1997. Lateral variations in mechanical properties of the Romanian external Carpathians: inferences of flexure and gravity modeling. Tectonophys. 282, 147–166.
Maţenco, L., Bertotti, G., Leever, K., Cloetingh, S., Schmid, S.M., Tărăpoancă, M., Dinu, C., 2007. Large-scale deformation in a locked collisional boundary: interplay between subsidence and uplift, intraplate stress, and inherited lithospheric structure in the late stage of the SE Carpathians evolution. Tectonics 26, TC4011. doi:10.1029/2006TC001951.
Nicolas, A., 1993. Why fast polarization directions of SKS seismic waves are parallel to mountain belts. Phys. Earth Planet. Inter. 78, 337–342.
Nicolas, A., Christensen, N.I., 1987. Formation of anisotropy in upper mantle peridotites — a review. In: Fuchs, K., Froidevaux, C. (Eds.), Composition, Structure and Dynamics of the Lithosphere–Asthenosphere System. : Am. Geophys. Un. Geodynam. Ser., vol. 16. pp. 111–123. American Geophysical Union, Washington D.C.
Oncescu, M.-C., Bonjer, K.-P., 1997. A note on the depth recurrence and strain release of large Vrancea earthquakes. Tectonophysics 272, 291–302.
Oncescu, M.-C., Mavrza, V., Rizescu, Z., Popa, M., 1999. The Romanian catalogue between 1984–1997. In: Wenzel, F., Lungu, D., Novak, O. (Eds.), Vrancea Earthquakes: Tectonics, Hazard and Risk Mitigation. Kluwer Academic, Dordrecht, pp. 43–47.
Pharaoh, T.C., 1999. Palaeozoic terranes and their lithospheric boundaries within the Trans-European Suture Zone (TESZ): a review. Tectonophysics 314, 17–41.
Plomerová, J., Babuška, V., Vecsey, L., Kouba, D., TOR Working Group, 2002. Seismic anisotropy of the lithosphere around the Trans European Suture Zone (TESZ) based on teleseismic body wave data of the TOR experiment. Tectonophysics 360, 89–114.
Radulescu, D.P., Sandulescu, M., 1973. The plate tectonics concept and the geological structure of the Carpathians. Tectonophysics 16, 155–161.
Radulian, M., Popa, M., 1996. Scaling of source parameters for Vrancea (Romania) intermediate depth earthquakes. Tectonophysics 261, 67–81.
Ribe, N.M., 1989a. A continuum theory for lattice preferred orientation. Geophys. J. Int. 97, 199–207.
Ribe, N.M., 1989b. Seismic anisotropy and mantle flow. J. Geophys. Res. 94, 4213–4223.
Ribe, N.M., Yu, Y., 1991. A theory for plastic deformation and textural evolution of olivine polycrystals. Geophys. J. Int. 94, 4213–4223.
Russo, R.M., Yu, Y., 2009. Subducted oceanic asthenosphere and upper mantle flow beneath the Juan de Fuca slab. Lithosphere 1, 195–205.
Russo, R.M., 2009. Subducted oceanic asthenosphere and upper mantle flow beneath the Juan de Fuca Slab. Lithosphere 1, 195–205.
Russo, R.M., submitted for publication. Source-side shear wave splitting and upper mantle flow beneath the Arakan slab, India–Asia–Sundaland triple junction region, Geosphere, submitted for publication.
Russo, R.M., Okal, E.A., 1998. Shear wave splitting in French Polynesia: evidence for small-scale heterogeneity related to the society hotspot. J. Geophys. Res. 103, 15,089–15,107.
Russo, R.M., Silver, P.G., 1994. Trench-parallel mantle flow beneath the Nazca Plate: results from seismic anisotropy. Science 263, 1105–1111.
Russo, R.M., Mocanu, V., Radulian, M., Popa, M., Bonjer, K.-P., 2005. Seismic attenuation in the Carpathian bend zone and surroundings. Earth Planet. Sci. Lett. 237, 695–709.
Saltzer, R.L., Gaherty, J.B., Jordan, T.H., 2000. How are vertical shear wave splitting measurements affected by variations in the orientation of azimuthal anisotropy with depth? Geophys. J. Int. 141, 374–390.
Sandulescu, M., 1998. Cenozoic tectonic history of the Carpathians. In: Royden, L.H., Horvath, F. (Eds.), The Pannonian Basin: A Study in Basin Evolution. Amer. Assoc. Petroleum Geol. Mem., vol. 45. Amer. Assoc. Petroleum Geol, Tulsa, OK, pp. 17–25.
Seghedi, I., Balintoni, I., Szakács, A., 1998. Interplay of tectonics and Neogene post-collisional magmatism in the intra-Carpathian region. Lithos 45, 483–497.
Seghedi, I., Downes, H., Szakács, A., Mason, R., Thirlwall, M., Roşu, E., Pécskay, Z., Márton, E., Panaiotu, C., 2004. Neogene–Quaternary magmatism and geodynamics in the Carpathian–Pannonian region: a synthesis. Lithos 72, 117–146.
Silver, P.G., 1996. Seismic anisotropy beneath the continents: probing the depth of geology. Annu. Rev. Earth Planet. Sci. 24, 385–432.
Silver, P.G., Chan, W.W., 1991. Shear wave splitting and subcontinental mantle deformation. J. Geophys. Res. 96, 16,429–16,454.
Sperner, B., Lorenz, F., Bonjer, K., Hettel, S., Mueller, B., Wenzel, F., 2001. Slab break-off: abrupt cut or gradual detachment? New insights from the Vrancea region (SE Carpathians, Romania). Terra Nova 13, 172–179.
Tărăpoancă, M., Bertotti, G., Maţenco, L., Dinu, C., Cloetingh, S.A.P., 2003. Architecture of the Focşani Depression: a 13 km deep basin in the Carpathian bend zone (Romania). Tectonics 22. doi:10.1029/2002TC001486.
Weidle, C., Widiyantoro, S., CALIXTO Working Group, 2005. Improving depth resolution of teleseismic tomography by simultaneous inversion of teleseismic and global P-wave traveltime data — application to the Vrancea region in southeastern Europe. Geophys. J. Int. 162, 811–823.
Weidle, C., Wenzel, F., Ismail-Zadeh, A., 2007. t^* - an unsuitable parameter to characterize anelastic attenuation in the Eastern Carpathians. Geophys. J. Int. 170, 1139–1150. doi:10.1111/j.1365-246X.2007.03441.x.
Wortel, M.J.R., Spakman, W., 2000. Subduction and slab detachment in the Mediterranean–Carpathian region. Science 290, 1910–1917.
Zhang, S., Karato, S., 1995. Lattice preferred orientation of olivine aggregates deformed in simple shear. Nature 375, 774–777.
Zhang, S., Karato, S., Fitzgerald, J., Faul, U.H., Zhou, Y., 2000. Simple shear deformation of olivine aggregates. Tectonophysics 316, 133–152.
Zhao, L., Jordan, T.H., Chapman, C.H., 2000. Three-dimensional Frechet differential kernels for seismic delay times. Geophys. J. Int. 141, 558–576.